

University of Memphis

University of Memphis Digital Commons

---

Electronic Theses and Dissertations

---

2021

**THE ACUTE EFFECTS OF CHRONIC TIME-RESTRICTED FEEDING  
AND EXERCISE ON MUSCLE IRON HOMEOSTASIS: A PILOT  
STUDY**

Matthew Brian Agoncillo Butawan

Follow this and additional works at: <https://digitalcommons.memphis.edu/etd>

---

**Recommended Citation**

Butawan, Matthew Brian Agoncillo, "THE ACUTE EFFECTS OF CHRONIC TIME-RESTRICTED FEEDING AND EXERCISE ON MUSCLE IRON HOMEOSTASIS: A PILOT STUDY" (2021). *Electronic Theses and Dissertations*. 2483.

<https://digitalcommons.memphis.edu/etd/2483>

This Thesis is brought to you for free and open access by University of Memphis Digital Commons. It has been accepted for inclusion in Electronic Theses and Dissertations by an authorized administrator of University of Memphis Digital Commons. For more information, please contact [khgerty@memphis.edu](mailto:khgerty@memphis.edu).

THE ACUTE EFFECTS OF CHRONIC TIME-RESTRICTED FEEDING AND EXERCISE ON  
MUSCLE IRON HOMEOSTASIS: A PILOT STUDY

By

Matthew Brian Agoncillo Butawan

A Thesis Submitted in Partial Fulfillment of the Requirements for

The Degree of Master of Science

Major: Nutrition

Concentration: Nutrition Science

The University of Memphis

May 2021

## ABSTRACT

*Background:* Iron is an essential mineral required for multiple metabolic actions in precise concentrations to avoid oxidative toxicity. Recent evidence suggests a novel nutrient-sensitive myokine, erythroferrone, may also act as a systemic iron regulator. This pilot study aims to investigate whether the duration of regular fasting lengths prior to exercise influences erythroferrone and muscle iron uptake. *Methods:* C57BL6 mice were divided into 3 groups with feeding windows relative to exercise: 1) *ad libitum*; 2) 6 hour window immediately post-exercise; 3) 6 hour window 5 hours post-exercise. Mice were exercised 5 days per week (Monday-Friday) for 8 weeks. Quadriceps erythroferrone and transferrin receptor-1 was assessed via PCR. Soleus sections were stained with a modified Perls' stain for iron content. *Results:* Erythroferrone and transferrin expression was not different between groups. Soleus iron content did not differ between groups. *Conclusion:* Fasting length prior to exercise does not seem to influence muscle iron content.

## TABLE OF CONTENTS

SECTION	PAGE
INTRODUCTION	
Overview.....	1
Biological Iron .....	2
Regulation of Iron Homeostasis.....	3
Modulation of Iron by Fasting and Exercise.....	4
METHODS	
Animals and Experimental Design .....	7
RNA Isolation and qPCR.....	8
Histology.....	9
Histological Image Processing.....	10
Statistical Analysis.....	11
RESULTS .....	12
DISCUSSION .....	13
REFERENCES .....	17
APPENDICES	
Appendix A: IACUC Approval .....	21
Appendix B: Stain Density Algorithm.....	22
FIGURES .....	26
TABLES .....	30

## LIST OF ABBREVIATIONS

ANOVA	Analysis of Variance
CTRP15	Complement component 1q/ Tumor necrosis factor-Related Protein-15
DMT1	Divalent Metal Transporter-1
ERFE	Erythroferrone
EPO	Erythropoietin
HSV	Hue-Saturation-Value
IRE	Iron Responsive Element
IRP	Iron Regulatory Protein
RGB	Red-Green-Blue value
SD	Standard Deviation
SEM	Standard Error Mean
TRF	Time-Restricted Feeding

## INTRODUCTION

Iron is an essential mineral with biological functions intertwined with bioenergetics and metabolism. Because excessive iron can cause oxidative damage, complex regulatory mechanisms must precisely control levels within a narrow homeostatic range. In fact, these regulatory mechanisms governing iron absorption and recycling are still being unraveled.

One puzzling example is the effect of fasting on these regulatory pathways. An acute fast has been shown to reduce systemic iron levels even in the presence of hypoferrremia. Regular fasts such as during Ramadan, are often cautioned in anemic populations due to the potential worsening of anemia; interestingly, being sedentary while undergoing a Ramadan fast seems to preserve hemoglobin levels in the presence of reduced erythrocyte counts whereas exercising while fasting reduces both hemoglobin and red blood cell counts (Hosseini & Hejazi, 2013). Time-restricted feeding, a form of intermittent fasting similar to Ramadan where daily food intake is restricted to a 4-8 hour window, is growing in popularity within fitness communities and may influence these regulatory pathways. Considering muscles have a high energy demand, this mineral may be of particular importance to muscle physiology, especially in the context when fasting is combined with exercise.

In 2012, a novel myokine, *myonectin*, was found in mice and characterized as C1q/TNF-related protein (CTRP)-15 (Seldin, Peterson, Byerly, Wei, & Wong, 2012). The expression of this myokine was found to be increased by exercise; differentially expressed in red and white muscles; and responsive to nutrient availability. In 2014, CTRP15 was later identified, and referred to as *erythroferrone* (ERFE), as a secretory product in bone marrow by another group of investigators that demonstrated its critical role as a hepcidin suppressor which subsequently

increases the bioavailability of iron for hemoglobin production by erythrocytes (Kautz et al., 2014).

Given the conceivable importance of iron to muscle physiology and the emergence of this “nutrient-sensitive” myokine as a potential regulator of iron homeostasis, this pilot study seeks to explore the chronic influences of a common dietary regimen, time-restricted feeding (TRF), in combination with aerobic exercise on muscle iron uptake outcomes.

### **Biological Iron**

Iron is an essential mineral and the most abundant *heavy metal* in the human body making up approximately 0.00006% by mass (Freese & Savage, 2012). Within the human body, as well as many other multicellular organisms, iron can be found incorporated into heme and hemoproteins, in various arrangements of iron-sulfur clusters, or in a free cationic state. Most commonly iron is found at the center of a heme cofactor (a coordination complex including a cyclic tetrapyrrole) most often associated with hemoglobin or myoglobin proteins. Iron-sulfur clusters are often recognized as redox centers of ferredoxins for electron transport. Though very uncommon due to its high reactivity, free cationic iron can be found in the ferrous ( $\text{Fe}^{2+}$ ) or ferric ( $\text{Fe}^{3+}$ ) state. For a more detailed overview of the biological forms and functions of iron, please see the review by Abbaspour et al. (Abbaspour, Hurrell, & Kelishadi, 2014).

While the contribution of iron to oxygen transport is fairly well understood (Pittman, 2011), its fundamental role in energy production should not be overlooked. Fe-S clusters are precisely arranged in ferredoxins of the electron transport chain so that electrons can spontaneously jump from cluster to cluster from lowest to highest redox potential in order to facilitate a  $\text{H}^+$  movement *against* its concentration gradient (Ramsay, 2019). Moreover, these Fe-S clusters serve as cofactors for the iron regulatory proteins (IRP1 and IRP2) (Cardenas-

Rodriguez, Chatzi, & Tokatlidis, 2018). IRP1 without its Fe-S cluster can affect translational activities by binding to iron-responsive-elements (IRE) contained on some mRNA which can either inhibit translation initiation or stabilize the nucleic acid and prevent degradation, depending on the location of the IRE. When IRP1 contains its Fe-S cluster, it has an aconitase activity which catalyzes the conversion of citrate, a key metabolic regulator, to isocitrate. Alternatively, IRP2 has recently been shown to modulate the switch from aerobic glycolysis to oxidative phosphorylation (H. Li et al., 2019). These functions underscore the importance of iron to cellular and tissue fuel selection—an important role for skeletal muscle (Hargreaves & Spriet, 2020), a primary consumer of metabolic fuels and contributor to systemic fuel levels.

Ultimately many of these functions of iron revolve around the iron's ability occupy a range of oxidation states and/or change affinity for diatomic oxygen. Given these central themes of biological iron, it is reasonable to assume iron plays a role in muscle physiology (Beard, 2001; Halon-Golabek, Borkowska, Herman-Antosiewicz, & Antosiewicz, 2019; Stugiewicz et al., 2016; van der Meer, van der Wal, & Melenovsky, 2019). Because free cationic iron is highly reactive and toxic at even low concentrations, systemic transportation of iron must be tightly controlled until ready to be used or stored by the tissue. Furthermore, there are no known excretion mechanisms (beyond hemorrhagic bleeding) so iron absorption and interorgan iron exchange must be tightly controlled.

### **Regulation of Iron Homeostasis**

Heme iron is overwhelmingly the most common form of iron. Iron can also be found in numerous other tissues throughout the body. That said, aside from bone marrow or the spleen, iron is also commonly found in liver, muscle, heart, and kidney (Navas & Córdova, 2000; Wakeham & Halenz, 1936). These metabolically active tissues may have also adapted

mechanisms to further fine-tune iron stores through resident macrophages (Winn, Volk, & Hasty, 2020). On the other hand, the brain has a high energy demand but does not readily store iron to prevent neurodegeneration likely fueled by the high reactivity. Considering the broad demand for iron throughout the body and narrow therapeutic window, a better understanding of iron regulation is critical to understanding this unique trace mineral.

Ingested iron is brought into intestinal cells most often through the divalent metal transporter (DMT1) as ferrous iron or through an incompletely understood mechanism involving the uptake of heme iron (Figure 1). Intracellular iron is stored either in ferritin or hemosiderin. Iron is exported out of cells through the ferroportin transporter. Systemic transport occurs while bound to transferrin. Extra-intestinal uptake of iron is most often through transferrin:transferrin receptor uptake. Systemic transport and absorption of iron is regulated through hepcidin, a liver hormone that results in the removal of ferroportin from the basolateral membrane. For a more detailed overview of iron regulation, please refer to the review by Anderson and Frazer (Anderson & Frazer, 2017).

While the liver is the most highly concentrated iron tissue, others have suggested muscle may contain similar amounts of iron when considering the large contribution of muscle mass to overall body weight (Torrance, Charlton, Schmanan, Lynch, & Bothwell, 1968).

### **Modulation of Iron Regulation by Fasting and Exercise**

Interest in intermittent fasting has increased over the last two decades, as much research has suggested numerous beneficial effects on metabolism, such as prevention of pancreatic fat deposition and improved insulin secretion (Quiclet et al., 2019); transcriptomic changes in the liver (Ng et al., 2019); and improvements to insulin sensitivity and skeletal muscle glucose uptake (Jones et al., 2020). Moreover, in the past decade, interest in intermittent fasting has

expanded into the mainstream, particularly within fitness communities (Rosenbloom, 2014). Intermittent fasting can be subclassified into alternate day fasting, time-restricted feeding, or a derivative of these. While there has been an abundance of health-related research centered around different fasting regimens, little research has investigated the effects on iron regulation which may have a contributory role in these processes, particularly within skeletal muscle.

While no studies were found investigating the effects of chronic intermittent fasting on iron regulation, many studies have examined the acute impact of fasting or starvation on this topic. However, results from many of these studies seem conflicting or counterintuitive. For example, one study suggests serum iron increases with fasting in healthy individuals (Nguyen, Buse, Baskin, Sadrzadeh, & Naugler, 2017)—a finding expected to be accompanied by reductions in hepcidin. However, another study found hepcidin levels to increase with fasting in humans (Troutt et al., 2012). In fact, other preclinical studies report similar findings in that despite iron deficiency in mice, fasting can cause increases in hepcidin expression (Y. Li, Booth, Feng, & Fleming, 2014; Vecchi et al., 2014). Recently Luo and colleagues suggested iron bioavailability may be increased by upregulating liver ferroportin expression and not significantly changing hepcidin expression levels with acute fasting (Luo et al., 2020).

With regards to acute exercise, hepcidin increases after exercise (Peeling et al., 2017; Peeling et al., 2014) and the magnitude of hepcidin response post exercise appears to be dependent on pre-exercise status of iron and circulating pro-inflammatory cytokines (Domínguez et al., 2018). Similar to fasting, no studies were found investigating the chronic effects of exercise training on iron regulation.

While most studies focus on the effects of fasting on the liver and the master iron regulator, hepcidin, a novel myokine may also play an important role in iron homeostasis. In

2012, Seldin et al. reported on the novel myokine, myonectin, as a nutrient-sensitive and exercise-induced muscle secretory product derived from the Fam132b gene (Seldin et al., 2012). In 2014, Kautz et al. reported on this same protein product derived from erythroblasts in the bone marrow and termed it erythroferrone—a key suppressor of hepcidin that allows for the increase in bioavailable iron for developing erythrocytes (Kautz et al., 2014). More recently, Little et al. investigated the effects of muscle erythroferrone deficiency using a knock-out mouse model on general hematogenous iron parameters including hemoglobin and hematocrit as well as liver hepcidin expression. Their findings suggested erythroferrone deficiency did not alter any hematogenous parameters or hepcidin levels under basal, non-stressed condition (Little et al., 2019). That said, this pilot study seeks to investigate the stress of fasting with exercise on erythroferrone expression and variables of muscle iron uptake.

## METHODS

### Animals and Experimental Design

The study was approved by the University of Memphis IACUC (Protocol# 0833) (Appendix A). Thirty-six male C57BL6 mice were purchased from Envigo (Indianapolis, Indiana) at 6 weeks of age. Mice were randomly pair caged in polycarbonate cages and given *ad libitum* access to water. Mice were separated into individual cages if mice observed fighting. Mice were housed in a temperature and light controlled room. Because mice are naturally nocturnal animals, the light:dark cycle was reversed so as to match active phases with investigators; lights were off (active phase) between 0600-1800.

Once received, mice underwent a three-week entrainment period during which they were given *ad libitum* access to food and water. At the end of the three-week entrainment period, mice were randomly placed into one of three intervention groups (n=12) wherein the time of food access relative to exercise was manipulated. That is, one group had *ad libitum* access to food (Control); one group only had access to food for a 6 hour period immediately after exercise cessation (TRF-Immediate); and one group only had access to food for a 6 hour period 5 hours after exercise cessation (TRF-Delayed).

Following the three-week entrainment period, mice ran five times per week (Monday through Friday) on a motorized treadmill (Exer 3/6; Columbus Instruments, Columbus, Ohio). The treadmill was set at a 10% incline for the daily exercise. Throughout the study, mice performed a 15-minute warmup during which they ran for 5 minutes at 5m/min, 5 minutes at 10m/min, and 5 min at 15m/min. During the first week of exercise, the speed was increased to 20m/min for only 30 minutes following the warmup. From the second week through the end of the study, mice ran at 20m/min for 45 minutes following the warmup. Exercise was performed in

the morning between 0600 and 0900. TRF-Delayed ran between 0600-0700, TRF-Immediate ran between 0700-0800, and Control ran between 0800-0900. An overview of the study design can be seen in Figure 2.

All mice were fed a growing rodent chow (AIN-93G, Research Diets, New Brunswick, New Jersey). This diet contained approximately 212 mg of ferric citrate per kg of food (Table 1). This was equivalent to approximately 48 mg Fe per kg of food which meets the dietary requirement needs for C57BL6J mice (Sorbie & Valberg, 1974) and the standards set forth by the American Institute of Nutrition 1977 (*Report of the American Institute of Nutrition ad hoc committee on standards for nutritional studies*, 1977).

To test the effects of time-restricted feeding windows relative to exercise, mice were split into three dietary intervention groups. The control group had *ad libitum* access to food, the TRF-Immediate group had access to food immediately after exercise between 0800 and 1400, and the TRF-Delayed group had access to food five hours after exercise between 1200 and 1800.

Mice were sacrificed following their normal exercise bout in a fasted state. Control mice had access to food prior to exercise; however, food was not returned post-exercise. Both fasting groups performed exercise in the fasted state, as usual, and neither group was allowed access to food post-exercise. Immediately following exercise cessation, mice were injected with Puromycin and sacrificed 30 minutes later. The left soleus muscle was stored in formalin. The right quadriceps muscle was snap frozen in liquid nitrogen. Tibia length was also recorded and used as a control for muscle size.

### **RNA Isolation and qPCR**

Expression for erythroferrone and transferrin receptor-1 was measured in quadriceps muscles. GAPDH was assessed as the housekeeping gene of this tissue. The erythroferrone

primer sequences were the same as those used by others (Seldin et al., 2012). Transferrin Receptor-1 and GAPDH primers were designed using the NCBI Primer Blast library and will be commercially produced (IDT, Coralville, IA). Primer sequences are listed in Table 2.

Tissues were homogenized in approximately 750µL Trizol. Total RNA was extracted from the homogenate by the addition of chloroform:isoamyl alcohol (24:1). RNA was resuspended in RNase free water, reprecipitated using sodium acetate and isopropanol, and washed with 75% ethanol three times. Isolated RNA was resuspended in water and quantified using a Nanodrop LITE (ThermoFisher Scientific, Waltham, MA). cDNA was prepared using 0.5µg of isolated RNA on a SimpliAmp thermocycler (A24812, Thermo Applied Biosystems, Waltham, Massachusetts, USA). cDNA was then mixed with forward and reverse primers for the intended target gene and Absolute Blue SYBR Green qPCR master mix. qPCR was performed on a QuantStudio 6 (Thermo Applied Biosystems, Waltham, Massachusetts, USA). The  $2^{\Delta\Delta Ct}$  method was used to determine changes in gene expression between intervention groups.

## **Histology**

Right soleus muscle was collected and placed in 10% buffered formalin phosphate before being processed with the following protocol: 70% ethanol 15 min, 90% ethanol 15 min, 100% ethanol 15 min, 100% ethanol 15 min, 100% ethanol 30 min, 100% ethanol 45 min, Histoprep 20 min, Histoprep, 20 min, Histoprep 45 min, paraffin wax at 60°C 30 min, paraffin wax at 60°C 30 min, paraffin wax at 60°C 45 min.

Processed tissues were then embedded in Paraffin using the Leica EG 1160 embedding unit. Embedded tissues were cut into 10 micrometer (µm) thick sections on the Microm HM 315 and placed onto a 45°C water bath. The sections were mounted onto charged uncoated glass slides. After an overnight drying process the tissue sections were stained with a modified

Prussian Blue staining procedure previously described (Sands, Leung-Toung, Wang, Connelly, & LeVine, 2016).

### **Histological Image Processing**

Images were acquired with a Zeiss AxioScope Imager M2 fixed with an Axiocam Mr5. After the whole section image was acquired, a 400um<sup>2</sup> red box was added to the image in the Zeiss software. The full image processing algorithm can be found in Appendix B. Briefly, the red channel was extracted and the number of pixels in the 400um<sup>2</sup> red box was computed from this image. A linear gradient with 20 unique red-green-blue (RGB) values between the darkest and lightest pixels contained within the tissue sample was created to compare images against.

A hue-saturation-value (HSV) threshold was applied to the original image in order to create a mask of the tissue section. The background of the threshold/masked image was strongly blurred to reduce the transmission of any background bubbles or artifact. The coordinates of the mask were used to bring matching coordinates from the original image into the new image that was processed. Once the new image was created containing the thresholded tissue section on a black background, the algorithm looped through all non-black pixels of a given image to obtain the RGB values. These RGB values were compared against the linear gradient created earlier in order to find the closest matching color in the linear gradient. The number of pixels closest matching each color in the linear gradient was counted and multiplied by a predefined factor.

The factor was scaled so that lighter colors weighed less than darker colors. The sum of the image weighted pixel colors were used to compute the stain intensity. Stain intensity was then divided by the tissue area to report as the stain density.

## **Statistical Analysis**

Gene expression data are presented as mean  $\pm$  SEM and tissue staining data are presented as mean  $\pm$  SD. A repeated measures ANOVA was used to assess differences across time and condition. A one-way ANOVA was used to compare across conditions. Tukey post hoc analysis may be used to examine interactions. GraphPad Prism 8 (San Diego, CA, USA) was used to analyze and graph all data with statistical significance set at  $p \leq 0.05$ .

## RESULTS

### Gene Expression

We examined whether 8-weeks of time-restricted feeding with varying durations of fasting prior to a regular exercise bout influenced post-exercise transcription of potential muscle iron uptake markers, specifically transferrin receptor-1 and erythroferrone in quadriceps. All subjects followed their typical feeding patterns prior to exercise; that being, the control group had food access until they began exercising, TRF-Immediate group began exercising on a 16-hour fast, and TRF-Delayed group began exercising on a 12-hour fast. Skeletal muscle tissue was collected approximately 30 minutes after completing their regular morning exercise with no subjects given food access post-exercise. There were no statistically significant differences in transferrin receptor-1 ( $p = 0.3427$ ) or erythroferrone ( $p = 0.4963$ ) expression between groups (Figure 3).

### Fasting Effects on Muscle Iron Staining

In order to estimate muscle iron content between groups, we attempted to compare the tissue staining 'density.' Briefly, a modified Perls' stain was used to identify ferric and ferrous iron in soleus muscles wherein darker staining indicates a higher presence of free iron. After algorithmically computing stain 'density' for each whole tissue section, we then sought to determine whether chronic time-restricted feeding combined with exercise altered muscle iron content. There were no statistically significant differences in staining density between groups ( $p = 0.8063$ ) (Figure 4).

## DISCUSSION

The present study sought to investigate whether the fasting length prior to exercise influences muscle iron uptake. After 8-weeks of chronic *ad libitum* or time-restricted feeding immediately post- or 5-hours post-aerobic exercise cessation, we examined the expression of muscle erythroferrone and transferrin receptor-1 as well as histological iron staining. This study failed to demonstrate any significant differences relating to the fasting length prior to an acute exercise bout on ERFE or TrfR-1 transcription in quadriceps muscle or total muscle iron staining. The premise of this pilot study was built off previous findings that indicated ERFE (or myonectin) was a myokine that was sensitive to the fasted or ‘re-fed’ state; the later finding of erythroferrone as a systemic iron regulator; and the curious effect of fasting on iron homeostasis.

In the initial ERFE characterization study, Seldin et al. found that skeletal muscle ERFE expression was greatly suppressed after a 12-hour fast in comparison to levels after a 2-hour refeeding period following a similar fast (Seldin et al., 2012). Surprisingly, our insignificant findings represent the opposite effect when combined with exercise in that our fasting groups had slightly higher ERFE expression levels (Figure 3). This may be due to the fact that the control group was sleeping and not eating prior to exercise and no group was allowed to eat post-exercise. Because the control group was sleeping, they may have been in a somewhat ‘fasted’ state they had not become accustomed to following exercise and just prior to sacrifice. However, this conjecture is based off the differing effects of acute and chronic fasting adaptations on hepcidin reported by others since acute and/or chronic fasting data on ERFE is lacking.

Most previous studies utilizing acute fasting periods similar to ours have reported liver hepcidin expression increases with acute fasts in mice (Y. Li et al., 2014; Vecchi et al., 2014)—a finding expected with low ERFE. Interestingly, one study validating a mass spectrometry-based

proteomics method used human plasma samples from an intermittent fasting trial (albeit more similar to alternate day fasting) and found plasma hepcidin abundance to be decreased after 8-weeks of fasting (Harney et al., 2019). In regards to fasting effects on muscle iron, one study did find that after a 24 hour fast, transferrin receptor expression decreases and heme oxygenase-1 expression increases in healthy, human skeletal muscle (Wijngaarden et al., 2014). This might suggest that rather than taking up additional iron, prolonged fasting skeletal muscle might attempt to recycle local iron stores, a role that might also contribute to muscle fiber type switching.

If ERFE levels had been different between our dietary groups, it could be assumed that liver hepcidin would be suppressed causing an increase in bioavailable iron (Kautz et al., 2014). In fact, a previous study reported hepcidin suppression and muscle iron accumulation after recombinant human erythropoietin (EPO) administration (Robach et al., 2009)—EPO was later found to be a major erythroblast ERFE inducer (Robach et al., 2020). An increase in bioavailable iron (bound to transferrin) would theoretically be taken up by cells in need of iron. That is, when intracellular iron levels are low, there would be decreased iron-sulfur clusters used as cofactors for IRPs which can stabilize the TrfR mRNA and increase the likelihood of TrfR synthesis (Wilkinson & Pantopoulos, 2014). The present study did not indicate there were any differences in total iron staining between groups; thus, it could be inferred that there would not be any differences in TrfR protein expression since TrfR-1 expression was also not significantly different between groups.

While aerobic exercise is known to induce muscle ERFE expression (Seldin et al., 2012), the only data regarding its effects on iron homeostasis are derived from a knockout mouse model and demonstrate no changes to hemoglobin or hematocrit levels (Little et al., 2019). Other

studies focusing on the effects of resistance exercise training on iron parameters use iron-deficient rat models. These studies indicate resistance training decreases iron absorption without affecting whole body iron content, a finding authors hypothesized to be caused by increased iron recycling (Fujii, Matsuo, & Okamura, 2014). This group also investigated the effects of post-exercise meal timing on hemoglobin concentration but found meal timing to have no effect on this outcome (Fujii, Matsuo, & Okamura, 2012). While our study used healthy mice, it is possible the use of an iron deficient population, like those mentioned previously, may have elicited more meaningful results. Especially since pre-exercise iron status seems to affect the EPO-ERFE-hepcidin axis after an intense aerobic exercise bout (Tomczyk et al., 2020).

There were several limitations to the present study: 1) the sample size of analyzed samples was small; 2) the aerobic conditioning of subjects was highly variable which may have affected expression levels as the regular exercise bout may have been more strenuous for some samples than for others; 3) our *ad libitum* group did not consume any food immediately post-exercise and prior to sacrifice; 4) the RNA expression was assessed on a mixed muscle type rather than a predominant white or red fiber; and 5) protein levels of TrfR-1 was not assessed.

That being said, while the current study did not uncover an association between the fasting length prior to exercise and muscle iron uptake, other studies do not exclude the possibility. Because iron status seems to be easily manipulated with fasting lengths, the combination of fasting with intense aerobic exercise may potentiate effects on the EPO-ERFE-hepcidin axis. As more research regarding the nutrient-sensitive erythroferrone emerges, a better understanding of the combined effects of fasting and exercise on iron regulation will be possible. Currently, research regarding erythroferrone as a myokine seem to be limited to its effects on modulating lipid stores and utilization (Little et al., 2019; Seldin et al., 2013) as well as insulin

resistance (Koohestani Sini, Afzalpour, Mohammadnia Ahmadi, Sardar, & Gorgani Firuzjaee; Pourranjbar, Arabnejad, Naderipour, & Rafie, 2018).

Future studies could be better designed to address whether an association between fasting length and exercise exists. Such a study might include a larger sample size, use of a run-to-exhaustion and voluntary wheel running to control for aerobic conditioning variance, and allowing a control group to consume immediately post-exercise. Additionally, a more quantitative measure of muscle iron content could be accomplished with a colorimetric assay and use of a Western Blot analysis would help determine whether there are differences in muscle TrfR-1 synthesis. Furthermore, it has been recently suggested that tissue macrophages may act to fine-tune systemic and tissue iron levels through sequestration (Winn et al., 2020). Because exercise induces some muscle damage, there would likely be iron-bound myoglobin that would need to be taken up to avoid oxidative damage once iron is released from myoglobin. This may be mediated by resident macrophages which may further be affected by fasting as others have demonstrated fasting-induced metabolic changes to adipose macrophages (Kim et al., 2017).

In conclusion, the present study failed to establish a relationship between fasting length prior to exercise and differences in muscle iron content. However, there are many avenues of research that could be utilized to more definitively conclude whether a relationship exists.

## REFERENCES

- Abbaspour, N., Hurrell, R., & Kelishadi, R. (2014). Review on iron and its importance for human health. *Journal of research in medical sciences: the official journal of Isfahan University of Medical Sciences*, 19(2), 164.
- Anderson, G. J., & Frazer, D. M. (2017). Current understanding of iron homeostasis. *The American journal of clinical nutrition*, 106(suppl\_6), 1559S-1566S.
- Beard, J. L. (2001). Iron biology in immune function, muscle metabolism and neuronal functioning. *The Journal of nutrition*, 131(2), 568S-580S.
- Cardenas-Rodriguez, M., Chatzi, A., & Tokatlidis, K. (2018). Iron–sulfur clusters: from metals through mitochondria biogenesis to disease. *JBIC Journal of Biological Inorganic Chemistry*, 23(4), 509-520.
- Domínguez, R., Sánchez-Oliver, A. J., Mata-Ordoñez, F., Feria-Madueño, A., Grimaldi-Puyana, M., López-Samanes, Á., & Pérez-López, A. (2018). Effects of an acute exercise bout on serum hepcidin levels. *Nutrients*, 10(2), 209.
- Freese, K., & Savage, C. (2012). Dark matter collisions with the human body. *Physics Letters B*, 717(1-3), 25-28.
- Fujii, T., Matsuo, T., & Okamura, K. (2012). The effects of resistance exercise and post-exercise meal timing on the iron status in iron-deficient rats. *Biological Trace Element Research*, 147(1-3), 200-205.
- Fujii, T., Matsuo, T., & Okamura, K. (2014). Effects of resistance exercise on iron absorption and balance in iron-deficient rats. *Biological Trace Element Research*, 161(1), 101-106.
- Halon-Golabek, M., Borkowska, A., Herman-Antosiewicz, A., & Antosiewicz, J. (2019). Iron metabolism of the skeletal muscle and neurodegeneration. *Frontiers in Neuroscience*, 13, 165.
- Hargreaves, M., & Spriet, L. L. (2020). Skeletal muscle energy metabolism during exercise. *Nature metabolism*, 1-12.
- Harney, D. J., Hutchison, A. T., Su, Z., Hatchwell, L., Heilbronn, L. K., Hocking, S., . . . Larance, M. (2019). Small-protein enrichment assay enables the rapid, unbiased analysis of over 100 low abundance factors from human plasma. *Molecular & Cellular Proteomics*, 18(9), 1899-1915.
- Hosseini, S. R. A., & Hejazi, K. (2013). The effects of Ramadan fasting and physical activity on blood hematological-biochemical parameters. *Iranian journal of basic medical sciences*, 16(7), 845.
- Jones, R., Pabla, P., Mallinson, J., Nixon, A., Taylor, T., Bennett, A., & Tsintzas, K. (2020). Two weeks of early time-restricted feeding (eTRF) improves skeletal muscle insulin and

- anabolic sensitivity in healthy men. *The American journal of clinical nutrition*, 112(4), 1015-1028.
- Kautz, L., Jung, G., Valore, E. V., Rivella, S., Nemeth, E., & Ganz, T. (2014). Identification of erythroferrone as an erythroid regulator of iron metabolism. *Nature genetics*, 46(7), 678.
- Kim, K.-H., Kim, Y. H., Son, J. E., Lee, J. H., Kim, S., Choe, M. S., . . . Lenglin, F. (2017). Intermittent fasting promotes adipose thermogenesis and metabolic homeostasis via VEGF-mediated alternative activation of macrophage. *Cell research*, 27(11), 1309-1326.
- Koohestani Sini, Z., Afzalpour, M. E., Mohammadnia Ahmadi, M., Sardar, M. A., & Gorgani Firuzjaee, S. The Effect of Aerobic Continuous Training on Myonectin, Insulin Resistance and Liver Enzymes in Rats with Nonalcoholic Fatty Liver Disease. *Annals of Applied Sport Science*, 0-0.
- Li, H., Liu, Y., Shang, L., Cai, J., Wu, J., Zhang, W., . . . Li, K. (2019). Iron regulatory protein 2 modulates the switch from aerobic glycolysis to oxidative phosphorylation in mouse embryonic fibroblasts. *Proceedings of the National Academy of Sciences*, 116(20), 9871-9876.
- Li, Y., Booth, G. R., Feng, Q., & Fleming, R. E. (2014). Hypoferremia of Fasting in Mice Is Associated with Increased Hepcidin and Decreased Erythroferrone Expression. In: *Am Soc Hematology*.
- Little, H. C., Rodriguez, S., Lei, X., Tan, S. Y., Stewart, A. N., Sahagun, A., . . . Wong, G. W. (2019). Myonectin deletion promotes adipose fat storage and reduces liver steatosis. *The FASEB Journal*, fj. 201900520R.
- Luo, Q., Hu, J., Yang, G., Yuan, X., Chen, Z., Wang, D., . . . Wang, G. (2020). Fasting increases iron export by modulating ferroportin 1 expression through the Ghrelin/GHSR1 $\alpha$ /MAPK pathway in the liver. *Biological Trace Element Research*, 1-11.
- Navas, F. J., & Córdova, A. (2000). Iron distribution in different tissues in rats following exercise. *Biological Trace Element Research*, 73(3), 259-268.
- Ng, G. Y.-Q., Kang, S.-W., Kim, J., Alli-Shaik, A., Baik, S.-H., Jo, D.-G., . . . Fann, D. Y.-W. (2019). Genome-Wide Transcriptome Analysis Reveals Intermittent Fasting-Induced Metabolic Rewiring in the Liver. *Dose-Response*, 17(3), 1559325819876780.
- Nguyen, L. T., Buse, J. D., Baskin, L., Sadrzadeh, S. H., & Naugler, C. (2017). Influence of diurnal variation and fasting on serum iron concentrations in a community-based population. *Clinical Biochemistry*, 50(18), 1237-1242.
- Peeling, P., McKay, A. K., Pyne, D. B., Guelfi, K. J., McCormick, R. H., Laarakkers, C. M., . . . Sharma, A. P. (2017). Factors influencing the post-exercise hepcidin-25 response in elite athletes. *European journal of applied physiology*, 117(6), 1233-1239.

- Peeling, P., Sim, M., Badenhorst, C. E., Dawson, B., Govus, A. D., Abbiss, C. R., . . . Trinder, D. (2014). Iron status and the acute post-exercise hepcidin response in athletes. *PloS one*, 9(3), e93002.
- Pittman, R. N. (2011). *Regulation of tissue oxygenation*. Paper presented at the Colloquium series on integrated systems physiology: from molecule to function.
- Pourranjbar, M., Arabnejad, N., Naderipour, K., & Rafie, F. (2018). Effects of aerobic exercises on serum levels of myonectin and insulin resistance in obese and overweight women. *Journal of medicine and life*, 11(4), 381.
- Quiclet, C., Dittberner, N., Gässler, A., Stadion, M., Gerst, F., Helms, A., . . . Schürmann, A. (2019). Pancreatic adipocytes mediate hypersecretion of insulin in diabetes-susceptible mice. *Metabolism*, 97, 9-17.
- Ramsay, R. R. (2019). Electron carriers and energy conservation in mitochondrial respiration. *ChemTexts*, 5(2), 9.
- Report of the American Institute of Nutrition ad hoc committee on standards for nutritional studies*. (1977). Retrieved from
- Robach, P., Gammella, E., Recalcati, S., Girelli, D., Castagna, A., Roustit, M., . . . Vergès, S. (2020). Induction of erythroferrone in healthy humans by micro-dose recombinant erythropoietin or high-altitude exposure. *Haematologica*.
- Robach, P., Recalcati, S., Girelli, D., Gelfi, C., Aachmann-Andersen, N. J., Thomsen, J. J., . . . Castagna, A. (2009). Alterations of systemic and muscle iron metabolism in human subjects treated with low-dose recombinant erythropoietin. *Blood, The Journal of the American Society of Hematology*, 113(26), 6707-6715.
- Rosenbloom, C. (2014). Popular diets and athletes: premises, promises, pros, and pitfalls of diets and what athletes should know about diets and sports performance. *Nutrition Today*, 49(5), 244-248.
- Sands, S. A., Leung-Toung, R., Wang, Y., Connelly, J., & LeVine, S. M. (2016). Enhanced histochemical detection of iron in paraffin sections of mouse central nervous system tissue: application in the APP/PS1 mouse model of Alzheimer's disease. *ASN neuro*, 8(5), 1759091416670978.
- Seldin, M. M., Lei, X., Tan, S. Y., Stanson, K. P., Wei, Z., & Wong, G. W. (2013). Skeletal muscle-derived myonectin activates the mammalian target of rapamycin (mTOR) pathway to suppress autophagy in liver. *Journal of Biological Chemistry*, 288(50), 36073-36082.
- Seldin, M. M., Peterson, J. M., Byerly, M. S., Wei, Z., & Wong, G. W. (2012). Myonectin (CTRP15), a novel myokine that links skeletal muscle to systemic lipid homeostasis. *Journal of Biological Chemistry*, 287(15), 11968-11980.

- Sorbie, J., & Valberg, L. (1974). Iron balance in the mouse.
- Stugiewicz, M., Tkaczyszyn, M., Kasztura, M., Banasiak, W., Ponikowski, P., & Jankowska, E. A. (2016). The influence of iron deficiency on the functioning of skeletal muscles: experimental evidence and clinical implications. *European journal of heart failure*, 18(7), 762-773.
- Tomczyk, M., Kortas, J., Flis, D., Kaczorowska-Hac, B., Grzybkowska, A., Borkowska, A., . . . Antosiewicz, J. (2020). Marathon Run-induced Changes in the Erythropoietin-Erythroferrone-Hepcidin Axis are Iron Dependent. *International journal of environmental research and public health*, 17(8), 2781.
- Torrance, J., Charlton, R., Schmaman, A., Lynch, S., & Bothwell, T. (1968). Storage iron in muscle. *Journal of clinical pathology*, 21(4), 495-500.
- Trout, J. S., Rudling, M., Persson, L., Ståhle, L., Angelin, B., Butterfield, A. M., . . . Konrad, R. J. (2012). Circulating human hepcidin-25 concentrations display a diurnal rhythm, increase with prolonged fasting, and are reduced by growth hormone administration. *Clinical chemistry*, 58(8), 1225-1232.
- van der Meer, P., van der Wal, H. H., & Melenovsky, V. (2019). Mitochondrial function, skeletal muscle metabolism, and iron deficiency in heart failure. In: Am Heart Assoc.
- Vecchi, C., Montosi, G., Garuti, C., Corradini, E., Sabelli, M., Canali, S., & Pietrangelo, A. (2014). Gluconeogenic signals regulate iron homeostasis via hepcidin in mice. *Gastroenterology*, 146(4), 1060-1069. e1063.
- Wakeham, G., & Halenz, H. F. (1936). *The distribution of iron in certain tissues of normal and anemic albino rats*: University of Colorado, Department of Chemistry.
- Wijngaarden, M. A., Bakker, L. E., van der Zon, G. C., 't Hoen, P. A., van Dijk, K. W., Jazet, I. M., . . . Guigas, B. (2014). Regulation of skeletal muscle energy/nutrient-sensing pathways during metabolic adaptation to fasting in healthy humans. *American Journal of Physiology-Endocrinology and Metabolism*, 307(10), E885-E895.
- Wilkinson, N., & Pantopoulos, K. (2014). The IRP/IRE system in vivo: insights from mouse models. *Frontiers in Pharmacology*, 5, 176.
- Winn, N. C., Volk, K. M., & Hasty, A. H. (2020). Regulation of tissue iron homeostasis: the macrophage “ferrostat”. *JCI insight*, 5(2).

APPENDICES

Appendix A: IACUC Approval



IACUC PROTOCOL ACTION FORM

To:	Richard J. Bloomer
From:	Institutional Animal Care and Use Committee
Subject:	Animal Research Protocol
Date:	December 20, 2018

The institutional Animal Care and Use Committee (IACUC) has taken the following action concerning your Animal Research Protocol No. 833

833 Impact of time restricted feeding and exercise on body composition and associated measures in male C57BL/6 mice
---

- Your protocol is approved for the following period:  
 From:  To:
- Your protocol is not approved for the following reasons (see attached memo).
- Your protocol is renewed without changes for the following period:  
 From:  To:
- Your protocol is renewed with the changes described in your IACUC Animal Research Protocol Update/Amendment Memorandum dated  for the following period:  
 From:  To:
- Your protocol is not renewed and the animals have been properly disposed of as described in your IACUC Animal Research Protocol Update/Amendment Memorandum dated

*Amy L. de Jongh Curry*  
 \_\_\_\_\_  
 Amy L. de Jongh Curry, PhD, Chair of the IACUC

*Karyl K. Buddington*  
 \_\_\_\_\_  
 Dr. Karyl Buddington, University Veterinarian and Director of the Animal Care Facilities

## Appendix B: Image Processing Algorithm

```
#import files to array and print array to confirm

import os
from pprint import pprint

files = []
for dirname, dirnames, filenames in os.walk('./test/'):
    #print path to all subdirectories
    for filename in filenames:
        #if statement used to avoid collecting file names from 'test' folder within 'test' folder
        if str(os.path.join(dirname, filename)[:8]) == "./test/g" or str(os.path.join(dirname, filename)[:8]) == "./test/r" or str(
            os.path.join(dirname, filename)[:8]) == ".DS_Store":
            pass
        else:
            files.append(os.path.join(dirname, filename))

files.remove('./test/.DS_Store')
pprint(files)
```

```
from mpl_toolkits.mplot3d import Axes3D
import matplotlib.pyplot as plt
from math import sqrt

def hex_to_RGB(hexcode):
    ''' "#FFFFFF" -> [255,255,255] '''
    #Pass 16 to the integer function for change of base
    return [int(hexcode[i:i+2], 16) for i in range(1,6,2)]

def RGB_to_hex(RGB):
    ''' [255,255,255] -> "#FFFFFF" '''
    #Components need to be integers for hex to make sense
    RGB = [int(x) for x in RGB]
    return "#"+"".join(["{:x}".format(v) if v<16 else
        "{:x}".format(v) for v in RGB])

def color_dict(gradient):
    ''' Takes in a list of RGB sub-lists and returns dictionary of
    colors in RGB and hex form for use in a graphing function
    defined later on '''
    return {"hex": [RGB_to_hex(RGB) for RGB in gradient],
            "r": [RGB[0] for RGB in gradient],
            "g": [RGB[1] for RGB in gradient],
            "b": [RGB[2] for RGB in gradient]}

def linear_gradient(start_hex, finish_hex="#FFFFFF", n=10):
    ''' returns a gradient list of (n) colors between
    two hex colors. start_hex and finish_hex
    should be the full six-digit color string,
    including the number sign ("#FFFFFF") '''
    # Starting and ending colors in RGB form
    s = hex_to_RGB(start_hex)
    f = hex_to_RGB(finish_hex)
    # Initialize a list of the output colors with the starting color
    RGB_list = [s]
    # Calcuate a color at each evenly spaced value of t from 1 to n
    for t in range(1, n):
        # Interpolate RGB vector for color at the current value of t
        curr_vector = [
            int(s[j] + (float(t)/(n-1))*(f[j]-s[j]))
            for j in range(3)
        ]
        # Add it to our list of output colors
        RGB_list.append(curr_vector)

    return color_dict(RGB_list)
```

```

def plot_gradient_series(color_dict, filename, pointsize=100, control_points=None):
    ''' Take a dictionary containing the color
    gradient in RGB and hex form and plot
    it to a 3D matplotlib device '''

    fig = mpp.figure()
    ax = fig.add_subplot(111, projection='3d')
    xcol = color_dict["r"]
    ycol = color_dict["g"]
    zcol = color_dict["b"]

    # We can pass a vector of colors
    # corresponding to each point
    ax.scatter(xcol, ycol, zcol, c=color_dict["hex"], s=pointsize)

    # If bezier control points passed to function,
    # plot along with curve
    if control_points != None:
        xcntl = control_points["r"]
        ycntl = control_points["g"]
        zcntl = control_points["b"]
        ax.scatter( xcntl, ycntl, zcntl, c=control_points["hex"], s=pointsize, marker='s')

    ax.set_xlabel('Red Value')
    ax.set_ylabel('Green Value')
    ax.set_zlabel('Blue Value')
    ax.set_zlim3d(0,255)
    mpp.ylim(0,255)
    mpp.xlim(0,255)

    # Save two views of each plot
    ax.view_init(elev=15, azim=680) #azim changed from 68 to 680
    mpp.savefig(filename + ".svg")
    ax.view_init(elev=15, azim=280) #azim changed from 28 to 280
    mpp.savefig(filename + "_view_2.svg")

    # Show plot for testing
    mpp.show()

grad_dict = linear_gradient("#f9ac63", "#521b10", 20)
#print(grad_dict)
plot_gradient_series(grad_dict, 'test', pointsize=100, control_points=None) #'test' is file name

#####Colors in the color gradient will be assigned a value between 1-20.
.....

#COLORS_dict is an empty list that will store hexcode values from gradient components created above
# for loop will extract RGB values and add hexcode color to COLORS_dict
COLORS_dict = []
reds = []
blues = []
greens = []
color = ()
index = 0
for key, value in grad_dict.items():
    if key == 'r':
        for i in grad_dict[key]:
            reds.append(i)
    if key == 'g':
        for i in grad_dict[key]:
            greens.append(i)
    if key == 'b':
        for i in grad_dict[key]:
            blues.append(i)

while index < 20:
    color = (blues[index], greens[index], reds[index])
    COLORS_dict.append(color)
    index += 1
    color = ()
#print(COLORS_dict)

#establishing a multiplier for each color
#lighter values hold a lighter multiplier - darker values weigh more heavily
COLORS_dict_multiplier = {}
mult = 1
for item in COLORS_dict:
    COLORS_dict_multiplier[item] = mult
    mult += 0.5
print(COLORS_dict_multiplier)

#find the absolute difference between one color (in image) and color in gradient scale
def closest_color(rgb):
    r,g,b = rgb
    color_diffs = []
    for color in COLORS_dict:
        cr, cg, cb = color
        color_diff = sqrt(abs(r-cr)**2 + abs(g-cg)**2 + abs(b-cb)**2)
        color_diffs.append((color_diff, color))
    return min(color_diffs)[1]

```

```

#this cell will be used to loop through array made above and extract RED color channel and write to new file in subfolder
#additionally will extract channel specific to tissue sample and write to new file in subfolder

import cv2
import numpy as np
from itertools import chain
from collections import Counter
from matplotlib import pyplot as plt

#Loop through array of image directories
for file in files:
    #setting up matplotlib lib to allow visualization of images as loop progresses
    #fig, axes = mpp.subplots(1, 6, figsize=(12, 6))
    #ax = axes.ravel()

    #read in the image
    img = cv2.imread(file, cv2.IMREAD_UNCHANGED)
    #ax[0].imshow(img)

    #####The red channel will be used to determine the number of pixels within the 400um2 standard square. #####
    #extract red channel
    red_channel = img[:, :, 2]
    #ax[1].imshow(red_channel)

    #convert original to grayscale
    gray_scale = cv2.cvtColor(img, cv2.COLOR_BGR2GRAY)
    #ax[2].imshow(gray_scale, cmap=mpp.cm.gray)

    #threshold red image
    ret, red_thresh = cv2.threshold(red_channel, 254, 255, cv2.THRESH_BINARY)

    #400um2 standard non-zero pixels
    standard = cv2.countNonZero(red_thresh)
    #print("Pixel standard: ", standard)

    #write red channel new image in subfolder 'red' as grayscale
    cv2.imwrite(os.path.join(os.path.realpath(file)[0:47] + '/red/' + file[7:]), red_channel)

    #####HSV thresholding will be applied to original images in order to create a mask of the tissue section. #####
    #defining range of tissue values
    BROWN_MIN = np.array([2, 130, 70], np.uint8) #H: 0-179 S&V: 0-255
    BROWN_MAX = np.array([170, 250, 250], np.uint8)

    #convert original to HSV image
    hsv = cv2.cvtColor(img, cv2.COLOR_BGR2HSV)

    #define threshold/make mask
    mask = cv2.inRange(hsv, BROWN_MIN, BROWN_MAX)
    output = cv2.bitwise_and(img, img, mask=mask)

    #binary thresholding
    ret, thresh = cv2.threshold(mask, 254, 255, cv2.THRESH_BINARY) #experiment with thresholding values
    #ax[3].imshow(thresh, cmap=mpp.cm.binary)

    #blur background
    blur = cv2.medianBlur(thresh, 13)
    blur2 = cv2.GaussianBlur(blur, (11, 11), -10)
    out = thresh.copy()
    out[mask > 0] = blur2[mask > 0]
    out = cv2.cvtColor(out, cv2.COLOR_GRAY2BGR) #BGR
    #ax[4].imshow(out, cmap=mpp.cm.binary)

    #overlay color image on top of mask coordinates
    color_out = cv2.bitwise_and(img, out, mask=mask)
    #ax[5].imshow(color_out)

    #save colored image to new file
    cv2.imwrite(os.path.join(os.path.realpath(file)[0:47] + '/blue/' + file[7:]), color_out)

    #####While working with the mask of the tissue section, cycle through the colored pixels of the original image. Each pixel of
    color_out_ar = np.array(color_out)
    #flatten 2D (W*H) pixel colors into 1D list of sublists
    flat_color_out_ar = []
    for sublist in color_out_ar:
        for item in sublist:
            flat_color_out_ar.append(item)

    #Output list initialization to find unique sublists
    Output = {}

    # Using Iteration
    for lis in flat_color_out_ar:
        Output.setdefault(tuple(lis), list()).append(1)
    for a, b in Output.items():
        Output[a] = sum(b)

    dark_pix_sum = 0
    area = 0
    true_area = 0
    close_color_list = []
    for key in Output:
        #below used to remove pixels approaching tissue section but not part of section
        if key[0] >= 35 and key[1] >= 35 and key[2] >= 35:
            c_col = closest_color(key)

```

```

        #print(c_col)
        close_color_list.append(c_col)
        area = area + Output[key]
        true_area = area * (400 / standard)
    else:
        dark_pix_sum = dark_pix_sum + Output[key]
    #print("Background: ", dark_pix_sum, "\n", "Area: ", true_area)

    #List_check = List(set(close_color_list))
    #print(List_check)

    #counting individual closest color pixels
    Output2 = {}
    # Using Iteration count number of unique closest pixels
    for lis in close_color_list:
        Output2.setdefault(tuple(lis), list()).append(1)
    for a, b in Output2.items():
        Output2[a] = sum(b)
    #print("Count of color pix: ", Output2)

    ##### Stain Intensity
    ##The number of pixels assigned to each color in the color gradient will be multiplied by the assigned value.

    #print("Multiplier: ", COLORS_dict_multiplier, "\n", "Color Count: ", Output2)
    im_pix_int = []
    for k in COLORS_dict_multiplier:
        if k in Output2:
            a = COLORS_dict_multiplier[k]
            b = Output2[k]
            pix_int = a * b
            #print(k, ": ", pix_int)
            im_pix_int.append(pix_int)
    stain_intensity = sum(im_pix_int)
    im_pix_int = []

    #print("Stain Intensity: ", stain_intensity)

    ##### Stain Density
    ##The products will be added and divided by the number of pixels in the continuous mask i.e. the area of the tissue section.
    stain_density = stain_intensity / true_area
    print(file[7:], "\t", stain_density, "\t area: ", true_area)

```

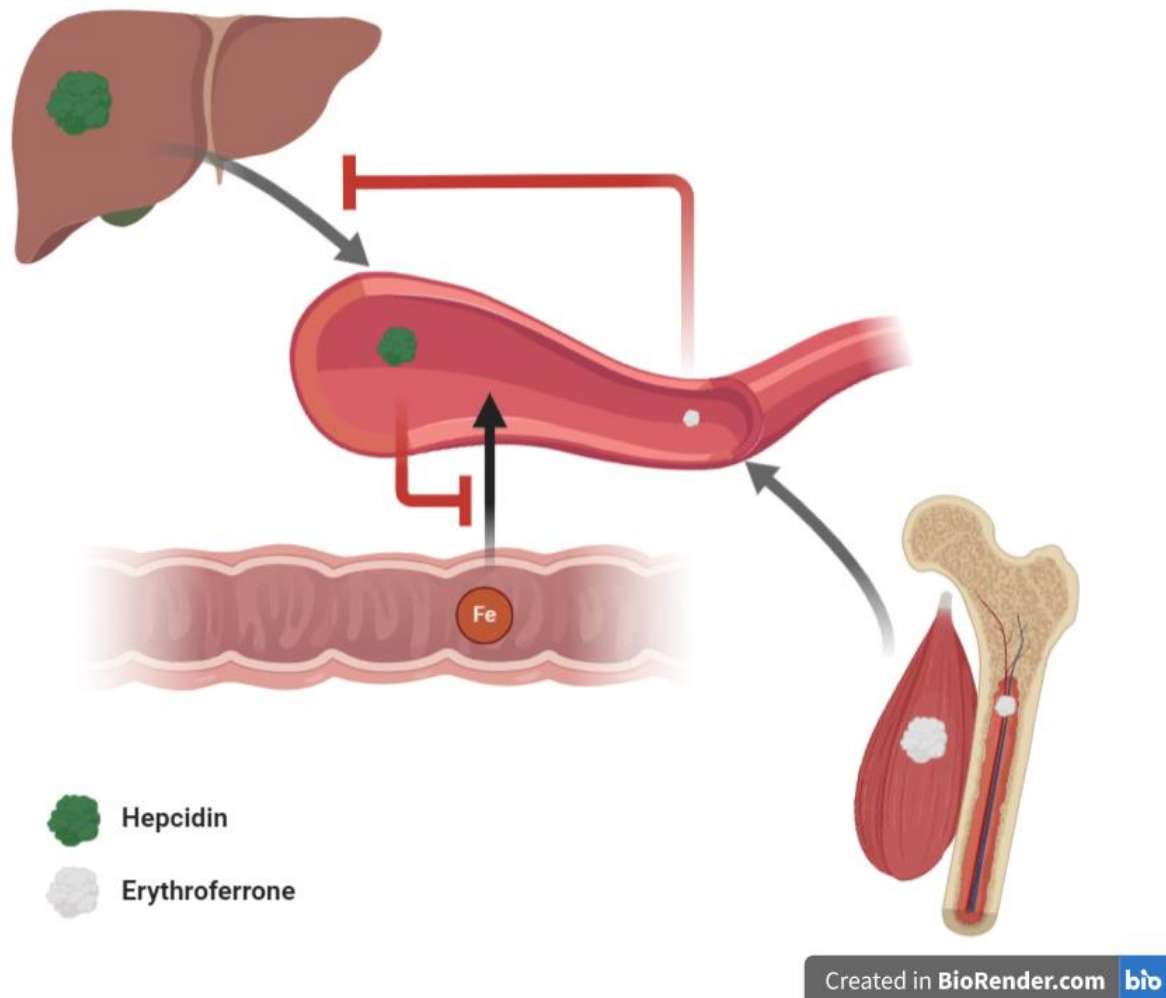


**Figure 1. Iron Absorption and Regulation.** An overview of the major path iron absorption mechanisms. Hepcidin inhibits the absorption of iron by preventing iron efflux from intestinal cells (as well as macrophages and hepatocytes). Erythroferrone suppresses hepcidin expression and secretion from hepatocytes, thereby increasing the bioavailability of iron.

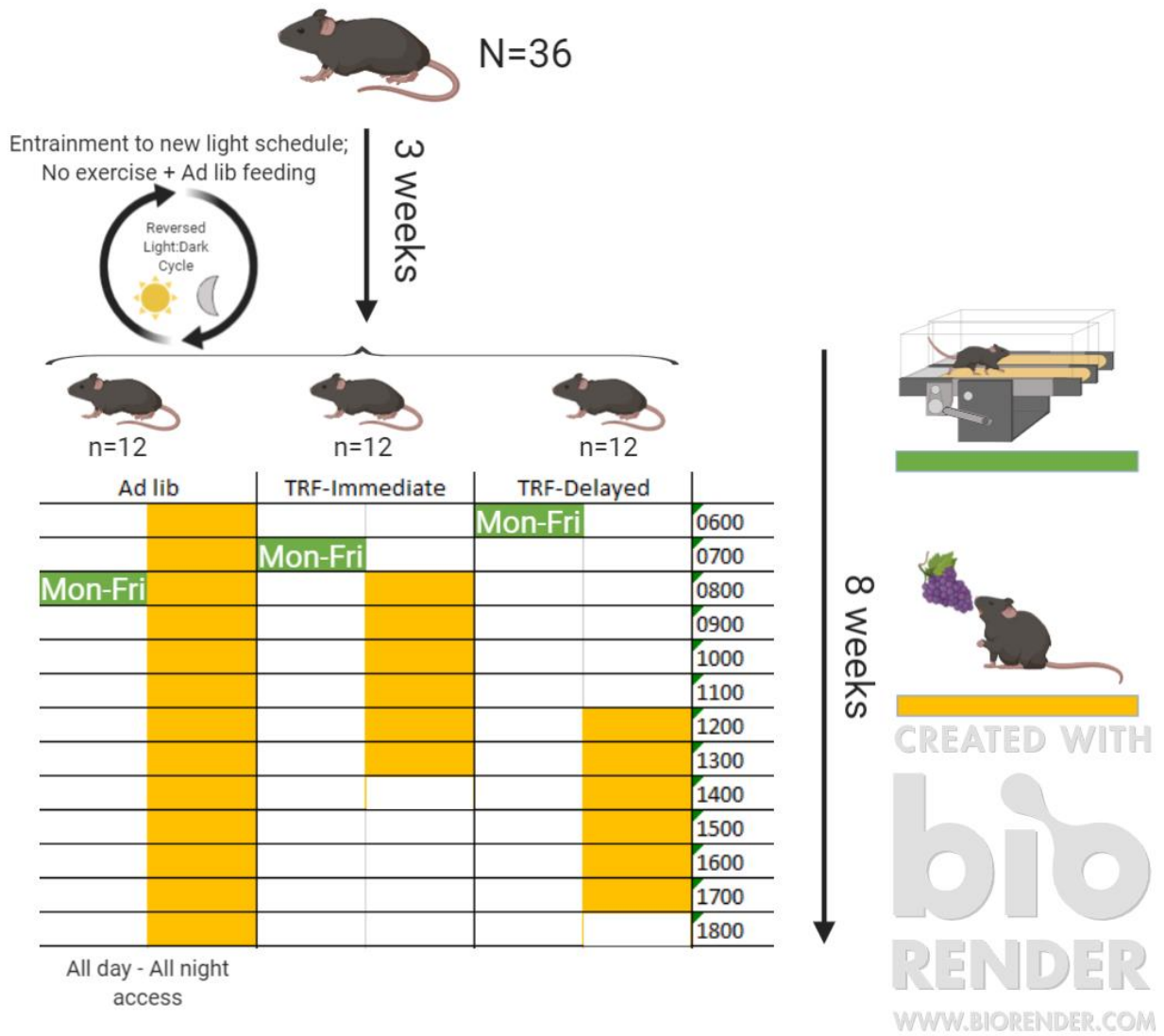


**Figure 2. Study Design.** An overview of the study design demonstrating the daily feeding patterns and weekly exercise of the mice.

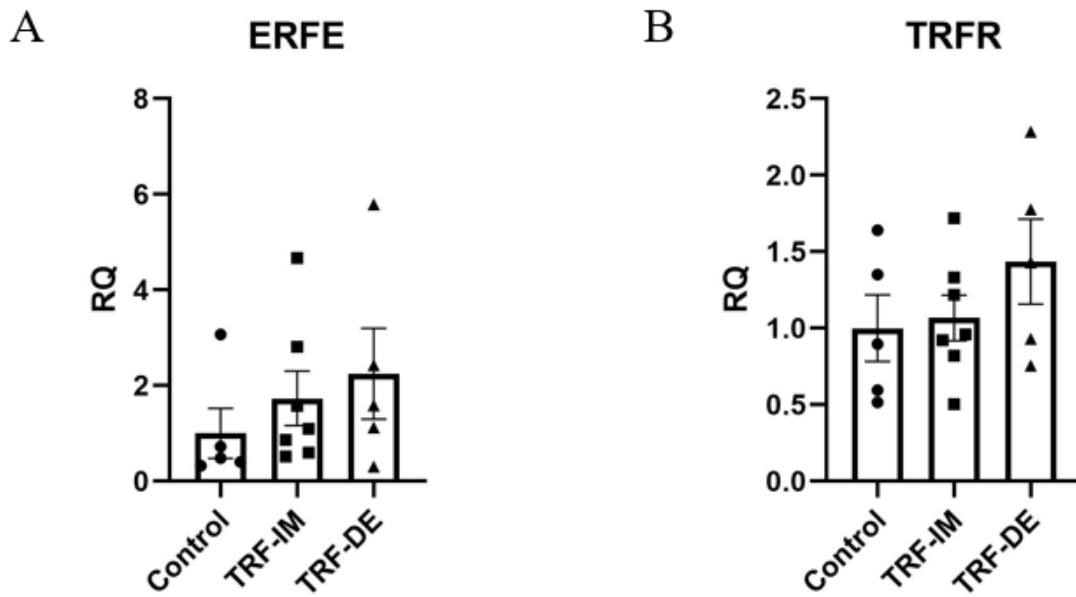


**Figure 3. Quadriceps muscle expression.** mRNA expression levels of A) erythroferrone and B) transferrin receptor-1 were measured in the quadriceps muscle. Data are presented as means  $\pm$  SEM. A one-way ANOVA was run on the  $2^{-\Delta\Delta C_t}$  of erythroferrone ( $p = 0.4963$ ) and transferrin receptor-1 ( $p = 0.3427$ ) to identify differences between groups.

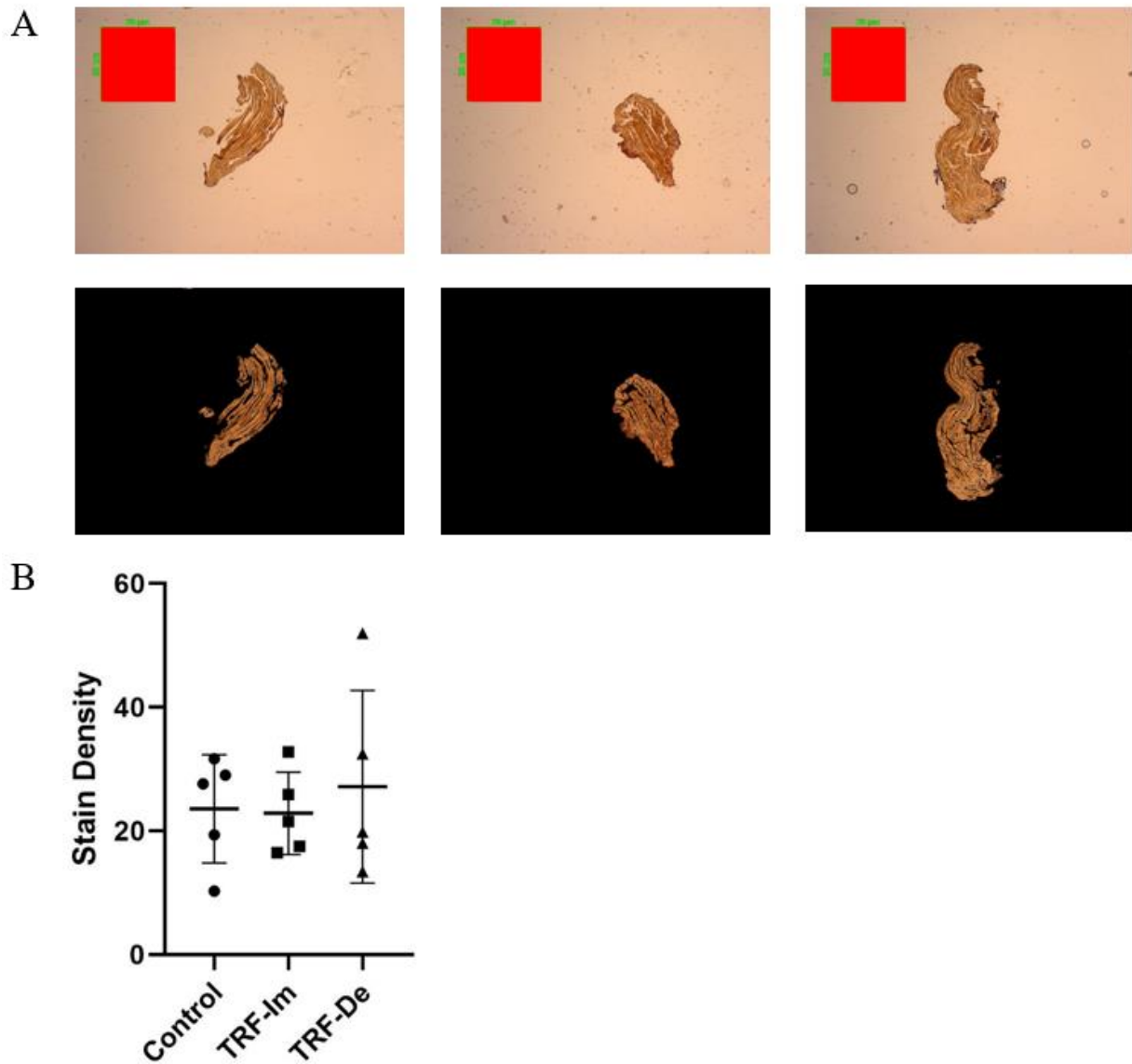


**Figure 4. Soleus Stain Density.** Whole slide samples stained with a modified Perls' stain to identify ferrous and ferric iron in soleus muscle. A) *Top*: Examples of slide images representing (from left to right) Control Group, TRF-Immediate Group, TRF-Delayed Group; *Bottom*: Processed image used to compute stain density. B) Stain density ( $p = 0.8063$ ) displayed as mean  $\pm$  SD.

**Table 1.** Diet per 1000g

<b>Class description</b>	<b>Ingredient</b>	<b>Grams</b>	
Protein	Casein, Lactic, 30 Mesh	200	g
Protein	Cystine, L	3	g
Carbohydrate	Starch, Corn	397.49	g
Carbohydrate	Lodex 10	132	g
Carbohydrate	Sucrose, Fine Granulated	100	g
Fiber	Solka Floc, FCC200	50	g
Fat	Soybean Oil, USP	70	g
Anti-oxidant	tert-Butylhydroquinone (tBHQ)	0.01	g
Mineral	Sucrose, Fine Granulated	7.73597264	g
Mineral	Calcium Carbonate, Light, USP	12.49487505	g
Mineral	Potassium Phosphate, Monobasic	6.859931401	g
Mineral	Sodium Chloride	2.5899741	g
Mineral	Potassium Citrate, Monohydrate	2.477275227	g
Mineral	Potassium Sulfate	1.63098369	g
Mineral	Magnesium Oxide, Heavy, DC USP	839.9916001	mg
<b>Mineral</b>	<b>Ferric Citrate</b>	<b>212.097879</b>	<b>mg</b>
Mineral	Zinc Carbonate	57.74942251	mg
Mineral	Sodium Metasilicate	50.74949251	mg
Mineral	Manganese Carbonate Hydrate	22.0497795	mg
Mineral	Copper Carbonate	10.499895	mg
Mineral	Chromium Potassium Sulfate	9.799902001	mg
Mineral	Boric Acid	2.799972	mg
Mineral	Sodium Fluoride	2.099979	mg
Mineral	Nickel (II) Carbonate	1.0499895	mg
Mineral	Lithium Chloride, anhydrous	0.699993	mg
Mineral	Sodium Selenate	0.3499965	mg
Mineral	Potassium Iodate	0.3499965	mg
Mineral	Ammonium Molybdate Tetrahydrate	0.3499965	mg
Mineral	Ammonium (meta)vanadate	0.3499965	mg
Vitamin	Sucrose, Fine Granulated	9.719203	g
Vitamin	Vitamin E Acetate, 50%	149.9985	mg
Vitamin	Niacin (a.k.a. B3)	29.9997	mg
Vitamin	Vitamin B12, 0.1% Mannitol	24.99975	mg
Vitamin	Biotin, 1%	19.9998	mg
Vitamin	Pantothenic Acid, d, Calcium (a.k.a. B5)	15.99984	mg
Vitamin	Vitamin D3, 100,000 IU/gm	9.9999	mg
Vitamin	Vitamin A Acetate, 500,000 IU/gm	7.99992	mg
Vitamin	Pyridoxine HCl (a.k.a. B6)	6.99993	mg
Vitamin	Riboflavin (a.k.a. B2)	5.99994	mg
Vitamin	Thiamine HCl (a.k.a. B1)	5.99994	mg
Vitamin	Folic Acid	1.99998	mg
Vitamin	Phylloquinone (a.k.a. Vitamin K1)	0.799992	mg
Vitamin	Choline Bitartrate	2.5	g

**Table 2.** Primers used

Erythroferrone	
<i>Forward 5' → 3'</i>	TGCTTGGATGCTGTTCGTCAA
<i>Reverse 5' → 3'</i>	CAGATGGGATAAAGGGGCTG
Transferrin Receptor-1	
<i>Forward 5' → 3'</i>	GGCGCTTCCTAGTACTCCCT
<i>Reverse 5' → 3'</i>	ATAGCCCAGGTAGCCACTCA
GAPDH	
<i>Forward 5' → 3'</i>	GTTGTCTCCTGCGACTTCA
<i>Reverse 5' → 3'</i>	TGCTGTAGCCGTATTCA